INTERNATIONAL JOURNAL OF AUTOMOTIVE AND MECHANICAL ENGINEERING
ISSN: 2229-8649 e-ISSN: 2180-1606
VOLUME 23, ISSUE 1, 2026, 13278 - 13294
DOI: https://doi.org/10.15282/ijame.23.1.2026.9.1007

RESEARCH ARTICLE

A comparative study of power and vibration signals for different tool pin sizes of friction stir welding

Maged Mustafa Abdulatef [1], Mohammad Kamil Sued[1]*, Ahmad Syahrazi Anuar[1], Tham Sook Chan[1], Muhammad Herman Jamaluddin[2], Ahmad Zaki Shukor[2], Mohd Khairi Mohd Zambri[2], Nor Azazi Ngatiman[3]

[1]Fakulti Teknologi dan Kejuruteraan Industri dan Pembuatan, Universiti Teknikal Malaysia Melaka, 76100 Durian Tunggal, Melaka, Malaysia

[2]Fakulti Teknologi dan Kejuruteraan Elektrik, Universiti Teknikal Malaysia Melaka, 76100 Durian Tunggal, Melaka, Malaysia

[3]Fakulti Teknologi dan Kejuruteraan Mekanikal, Universiti Teknikal Malaysia Melaka, 76100 Durian Tunggal, Melaka, Malaysia

Abstract – Process signals play an important role in revealing weld formation, reflecting the interaction between mechanical mixing and process parameters. This study focuses on how different tool pin lengths and material thicknesses influence the signals generated during friction stir welding of AA6061. Three pin lengths that were 2 mm, 4 mm, and 6 mm were tested on plates with thicknesses of 4 mm, 6 mm, and 8 mm (made by stacking two 4 mm plates). Spindle speed of 1200 RPM and a traverse speed of 50 mm/min were constant. Shorter pins cannot fully penetrate thicker plates in a single pass; therefore, welding was performed in dual passes, top and bottom, to complete the joint. During welding, power consumption and vibration signals were recorded. Data collected from the bottom side were used for detailed analysis, as the top pass helped hold materials before full penetration. The signals were analyzed using the Fast Fourier Transform, and standard deviation and defect accuracy were calculated to evaluate the weld condition. The findings show that the 2 mm pin achieved the highest defect accuracy of 90.63% based on power signals, while the 6 mm pin achieved the highest accuracy of 85.10% based on vibration signals. Larger vibration standard deviations from the 6 mm pin indicate energetic material stirring. Hardness results suggest that the 4 mm pin provides the most favorable material consolidation. These outcomes highlight that pin length and plate thickness significantly affect process signals, making them crucial variables for real-time weld quality monitoring and optimization.

Article history
Received : 14th May 2025
Revised : 5th Nov. 2025
Accepted : 23rd Dec. 2025
Published : 12th Mar. 2026

Keywords
Friction stir welding
Pin length
Material Thickness
Fast Fourier Transform
Process parameters

1. Introduction

Friction stir welding (FSW) is a solid-state joining method [1] developed by W. Thomas at the Welding Institute in the United Kingdom in 1991 [2]. It is a process that uses a non-consumable, rotating tool comprising a shoulder and a pin inserted into the metal for stirring the material. A joint is created behind the tool[3]. The tool plastically deforms the workpiece material without melting, producing high-quality welds with minimal flaws. The quality of welds, such as weld strength, hardness, and elongation, produced by FSW, is one of the primary benefits of the process (in contrast to fusion welding techniques). However, identifying weld conditions is expensive because it requires destructive testing techniques [4]. Identifying flaws is a challenging task, as most defects are internal or subsurface, where visual inspection is impractical [5]. However, evaluating the weld condition of a friction stir weld can be simplified relatively quickly by relying on process signal measurement and analysis. This technique has demonstrated the potential to identify flaws introduced during welding. Most of these studies focus on monitoring tool force during mixing, material type, and welding sensor position[4]. For example, in B. Das et al.'s study [5], sensor data were effectively used to monitor the welding process and identify defect occurrences. These studies have focused mostly on welding force measurement. However, to date, only a few studies have examined how vibration and power signals influence FSW welding to identify weld conditions and detect defects. Early work by Teresa et al. [6] used a power-measuring system connected to the motor accelerometer, along with temperature measurement, to monitor the FSW process. They found that peaks recorded by temperature caused alterations in both acceleration and power consumption when flash and surface defects occurred. This means that temperature and vibration measurement data can be used to identify the weld condition. In other fields, like machining, vibration measurement is common. For instance, a study involving vibration can be found in the previous work conducted by Kouguchi and Yoshioka [7]. They suggested a way to track estimated cutting forces and vibrations for high-speed cutting. The study separates these two signals by using an approximation of sequential quadratic regression. However, their study combined force and vibration data. Therefore, this paper aims to investigate the feasibility of selecting power and vibration measurements for condition monitoring.

The previous study's investigation shows promising results for detecting process conditions. However, the challenge is to analyze the measurement data. Different data processing approaches, such as Fast Fourier Transform FFT, Continuous Wavelet Transform CWT, Discrete Wavelet Transform DWT, and Wavelet Packet Transform WPT, could be utilized to extract various features of the welding for identifying various defects. Using time-frequency analysis and sensor-based signal acquisition methods, this investigation aims to establish a fundamental understanding of how signal features reflect weld quality. Extracting appropriate features from signals using signal processing technology is a vital foundation for weld formation identification [8]. In feature selection methods, the goal is to determine the most influential

*CORRESPONDING AUTHOR | Mohammad Kamil Sued | ✉ kamil@utem.edu.my

predictors among the categorization features[9]. These features from the signal would then be used to pinpoint variations during the welding process, which can aid in process control and, when necessary, defect detection [10]. Statistical features, including variance and the squared errors of the detail coefficients, are applied to the processed zone to identify defect locations[11]. Feature detection can be performed based on the machine's (a) vibration signals or (b) power consumption data. Therefore, a change in current or power consumption by a motor occurs when the welding process condition changes during the machining process. Based on the review, Axinte and Gindy investigated the utility of spindle power consumption during milling to monitor cutting tool condition, a critical process-related parameter influencing weld quality. The authors used both the cutting power calculated from prevailing forces and torque, and the spindle power for this purpose. They observed that the spindle power was insufficient to reliably identify the tool condition when a tooth chipped off. Nonetheless, spindle power showed a strong association with tool wear [10]. Moreover, vibration can reveal insights into the welding defect through feature extraction during the welding experiment. This feature can visualize the captured defect signal caused by converting the machine specimen vibration into a frequency signal. Balachandar et al. studied vibration analysis approaches for Al alloy experimentation. Signals were captured for good and faulty conditions of the FSW tool. Statistical information, such as the mean, median, and standard deviation, was extracted from the raw vibration signatures, and the features were selected. A large number of features were used to select the contributing features. However, the purpose of this work was to use machine learning to monitor the FSW tool's state [12].

In the recent decade, many investigations have focused on the relationship between defects and the parameters characteristic of FSW. The defect in the joint should result in a change to the proper tool geometry. Furthermore, the quality of welds produced by FSW depends on this complex material flow and the metal's ability to fill and mix behind the pin as it passes through the weld [3]. Some process parameters, including tool design, rotational speed, traverse speed, and axial force, affect the overall quality of weld material flow. An experimental study has been conducted to investigate the effects of rotational tool speed and pin profile on the yield strength and elongation of weld joints. The impact of tool design on mechanical properties and microstructure in friction stir welding was analyzed, revealing that material flow and weld joint quality are primarily influenced by tool geometry and process parameters [13]. Process parameters are one of the methods to regulate the quality of material that can be welded using FSW. The primary practical challenge in combining varying amounts of weldable aluminum is that each alloy, represented by grades or families, has its own strengths and weaknesses to meet specific requirements [14]. Moreover, tool pin size plays a crucial role in determining vertical material flow, thereby impacting mechanical mixing and machine condition, such as vibration. The pin length affects the material flow, resulting in defects in the weld. It is important to note that inappropriate interaction between the base materials and the formation of intermetallic tooling are major factors that promote the creation of defective welds[15]. Spindle and travel speeds will ensure material is ready for stirring, thereby preventing weld defects. Defect formation during welding reduces weld strength. The reason is the material flow during stirring [16]. Several common types of defects in the welded zones include wormholes, scalloping, ribbon flash, surface lack of fill, nugget collapse, and surface galling[2]. Therefore, selecting process parameters is crucial to preventing weld degradation. The material structural integrity of the weld is fundamentally related to the geometry and local mechanical properties of the defective zones[17]. Liu et al. discovered that the microstructure along the material flow path was characterized and analyzed by accounting for strain, strain rate, and temperature simultaneously[18]. Based on the review, the optimized parameter found from previous research for the aluminum 6xxx alloy family is shown in Table 1 and Figure 1. Based on the obtained data, the selected welding and spindle speeds for the Al 6xxx series are 30–100 mm/min and 800–1600 rpm, respectively. As a result, an appropriate strategy is needed to implement monitoring techniques for weld quality assessment.

Table 1. Parameter specification of the 6xxx

Parameter / No	Rotational Speed RPM	Welding Speed mm/min	Force KN	Tensile Strength MPa	Reference	Material
1	920	78	7.2	160.5	[19]	6061-T4
2	1000	550.2	4.5	194.7	[20]	6063-T6

Consequently, while pin size variations and workpiece thickness can have a major impact on the stirring action, material integration, and the joint's mechanical characteristics, a definitive correlation between the tool pin sizes, the workpiece material thickness, which imposes varying energy requirements, and the resultant in-process signal patterns to identify weld process flaws remains unestablished. Therefore, to detect process anomalies or flaws, statistical feature analysis and the Fast Fourier Transform (FFT) are two signal-processing techniques that extract relevant characteristics from these signals. These characteristics offer a promising approach for predicting structural integrity and weld quality when correlated with mechanical test results. In this paper, the effect of the FSW pin tool length on different plate thicknesses will be investigated using a current clamp meter and a vibration meter over a short data-collection period. The main objective of the presented work is to bridge this gap by using the process signal to quantify weld formation via its pattern. Three different tool pin sizes are used to evaluate tool pin geometry on AA6061 Aluminum alloy. The Fast Fourier Transform (FFT) is used to analyze power and vibration signals to identify the possibility of extracting a pattern in the measured power and vibration data, in conjunction with mechanical and microstructural testing outcomes. The results could help develop intelligent, sensor-integrated FSW systems that can predict defects and ensure real-time quality and structural integrity monitoring.

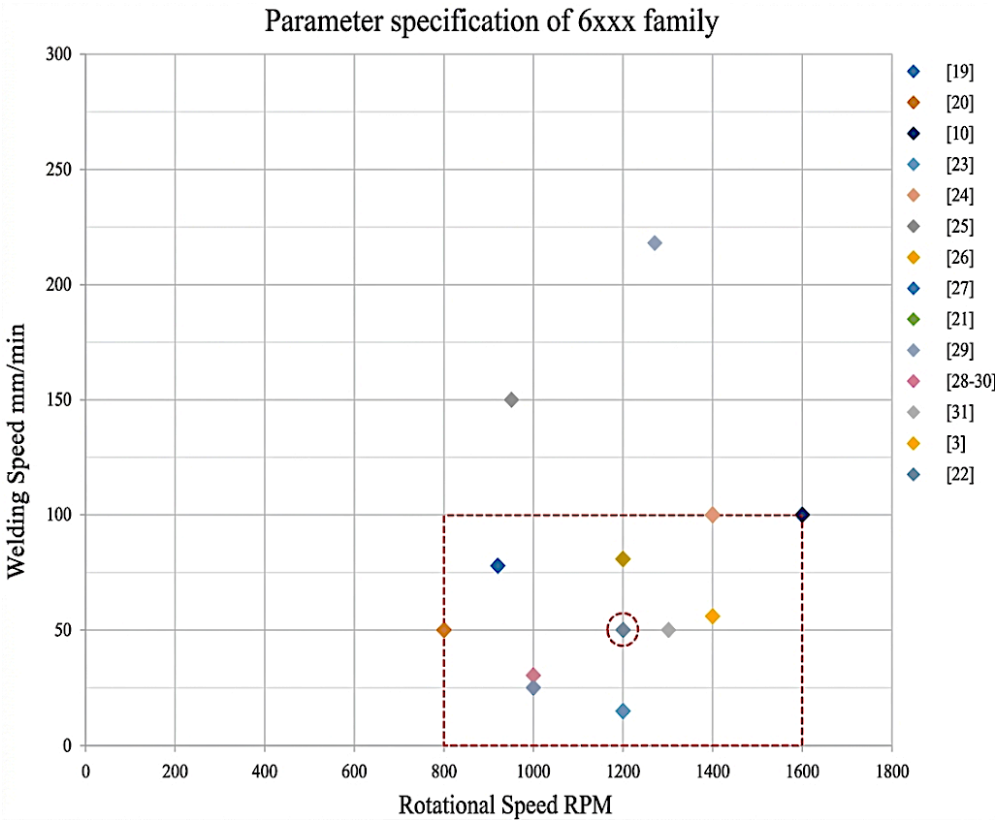

Figure 1. Plot of previous parameter sitting studies[[3], [10] , [21-31]]

2. Materials and Methods

2.1 Experimental Setup

An HMC1007-2D computer numerical control (CNC) FSW milling machine with a rigid clamping fixture and a CNC system is used for the welding experiments. The base material consists of two similar aluminum alloys of the 6061-T6 family, with thicknesses (t) of 4, 6, and 8 mm, prepared for welding. The 8 mm material thickness is the combined (overlapped) thickness of two 4 mm plates. The aluminum alloy plates' dimensions are 240 x 120 x t mm in butt joint configuration, with the tool rotated anticlockwise as illustrated in Figure 2. For the welding tool, 2 mm, 4 mm, and 6 mm pin lengths are used. Each pin length has a different shoulder diameter: 12, 14, and 16 mm, respectively. The pin has features of a tapered shape with three flats and threaded faces. During welding, power and vibration sensors are used to record input data via a data acquisition system mounted on the CNC milling machine, as shown in Figure 3. In this study, the selected parameters are a rotational speed of 1200 RPM and a welding speed of 50 mm/min, with the plunge depth adjusted based on plate thickness and an axial force of 5 kN, corresponding to 410 kg. This falls within the stated range, summarized from the literature. To track process behavior, an accelerometer was installed close to the weld zone to record vibration data, and a clamp-type current sensor was connected to the spindle motor line to record power signals. For every run, the data acquisition system was calibrated, and all signals were sampled at a high rate to maintain frequency-domain and time-domain detail.

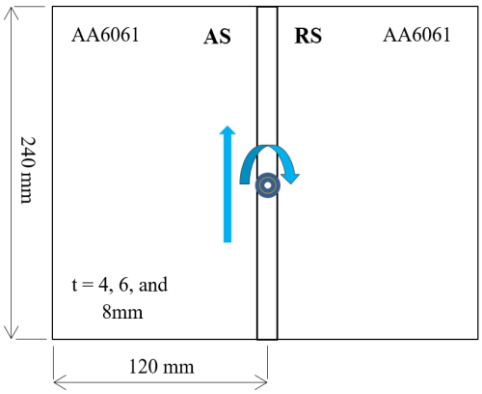

Figure 2. The sample joint setup

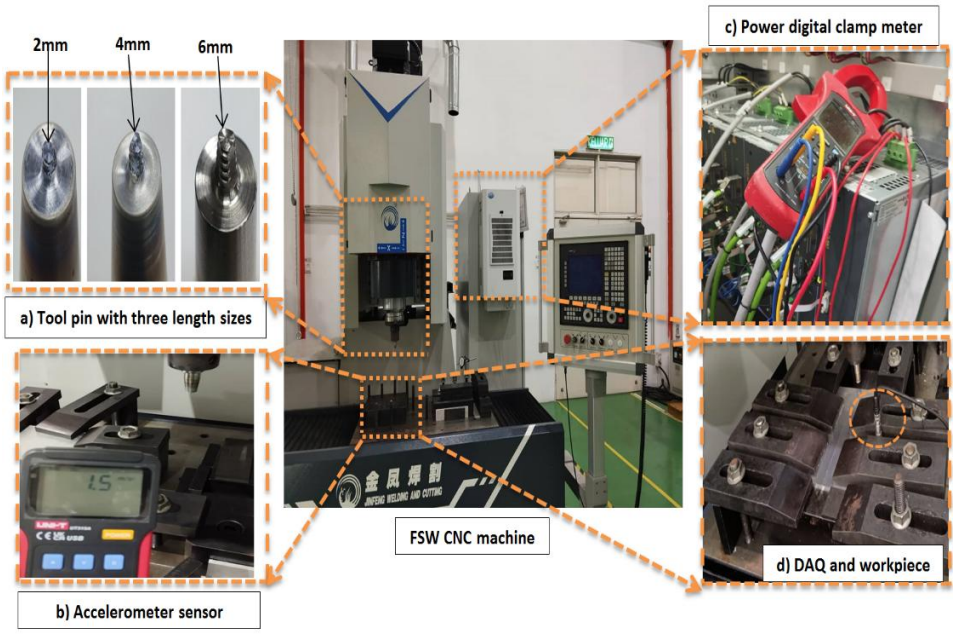

Figure 3. FSW machine set up and sensor position (a) Tool holder (b) A tri-axial accelerometer in Z-axis (c) Three-phase power supply line to the spindle motor (d) USB-6361 at a sampling rate of 10 kHz

2.2 Data acquisition and weld quality analysis

The process signal analysis starts with setting the tool parameters before the interaction between the selected material to be welded and the selected tool. During the welding, a power and vibration meter was used to measure the real-time data, as shown in Figure 3. The power signal is captured using an in-line power digital clamp meter sensor (UNI-T UT 233) with a sampling rate of 0.01 k ~600 kW, and accuracy of ±(1.5% +10 value) when frequency bandwidth at 50~60H z, while vibration signals are obtained using an accelerometer sensor (UT315A) with a sampling rate 0.1–199.9 m/s², and accuracy of ±5% ±0.2 m/s², when frequency bandwidth at 10 Hz–10 kHz. In order to identify the pin tool size weld formation, which offers an energy-efficient welding operation, the power input (P_{Input}) to the spindle motor is calculated from the line current using the following equation (1) [13]. Where, V_L is line voltage, I_L is line current, and Cosθ is the induction motor power factor of value 0.77.

$$P_{input} = [\sqrt{3}\, V_L\, I_L \cos\theta\,] / 1000 \quad (1)$$

The MATLAB software is used to analyze the measured power and vibration values. The power of the spindle motor was recorded throughout the entire route welding process using a calibrated power sensor in kilowatts (kW). Similarly, the vibration signal was measured in (m/s^2) and filtered to reduce noise while maintaining signal features. The data are analyzed using the Fourier transform (FT) for determining the power and vibration signals. A rectangular window was employed in the time- and frequency-domain analysis. The signal filtering is the second step after visualizing the signal. The filtering could be in (rapid design, fast iterations, streamlined design flow, or design for implementation). In this case, the streamlined design flow is chosen to explore design methods and analyze responses visually. The high-frequency component must be removed to provide a clearer view for analyzing the signal. De-trending the signal, low-pass filtering, and delay compensation are the steps to get the final visualization. Because the maximum frequency is low, the cut-off signal will be in the range that eliminates the high-frequency signal. The interactive method is used to filter and visualize the signal. The low-pass filter has been chosen using the IIR design method. The plot of the frequency analysis will define the characteristics of the signal in time-series or frequency analysis. Using the generation data functions to create data simulating the behavior of the signal is represented over time in the time domain and in the frequency domain window, in hertz. The FT is used to extract frequency components and assess the impact of tool pin size on the signal visualization. The change in the signal's amplitude and trend in defective cases is a clear indication of a process anomaly during the welding operation. Likewise, the vibration signal is intended to reveal the defect across different tool lengths. When welding starts, the defect in the material is reflected in the sensor measurements. This frequency pulse is to give the amplitude of unusual phase frequencies that indicate a defect. The first measurement displays power and acceleration over time in the time-domain signal. FFT analysis is also one of the most used techniques for defect diagnosis for vibration signals [32]. The FFT formula is given in Eq. (2), where f(t) represents the time domain signal and f(ω) represents the frequency domain signal. Furthermore, the obtained frequency components can be represented with a sine function including three variables: amplitude (A), frequency (ω), and phase (φ) [8].

$$F(\omega) = F\big(f(t)\big) = \int_{-\infty}^{+\infty} f(t) e^{-i\omega t} dt \quad (2)$$

$$F(\omega) = A \cdot sin(2\pi \cdot \omega \cdot t + \varphi) \quad (3)$$

The FSW vibration characteristics are then identified for different tool sizes. These features are filtered out of the signal's noise and interference. Then the frequency domain could be analyzed for a harmonic or frequency signal, as equations (4) and (5) follow[32] [8].

$$S_x(\omega) = \int_{-\infty}^{+\infty} R_x(\tau) e^{-i\omega t} d\tau \tag{4}$$

$$D = \frac{A(n) - A(2n)}{A(n)} \tag{5}$$

where D is a parameter of the first and second harmonics, A(n) and A(2n) are the first and second harmonic amplitudes. Consequently, the defect ratio range between the peaks is represented. Further statistical analyses are necessary because some data were lost or masked in the time domain, and statistical parameters such as mean, standard deviation, and kurtosis were computed to quantify signal behavior. The statistical frequency signals data represent all important features and information for the quality effect. The correlation between the formation of internal and external defects offers a crucial tool for evaluating quality. The preliminary identification of defect areas was selected based on visual inspection of the external welding path. Excessive flash defects within the weld path can serve as evidence of an internal defect for subsequent correlation with the FFT signals. The quality of the weld is related to the validation of defects and mechanical properties. The size of the pin affects joint strength, with a larger pin yielding greater strength than a smaller one in the first data examination. For this reason, a comparison of the pin tool size for different thicknesses of 6xxx AA material is conducted in this research. Figure 4 shows a plot of the overview process analysis flow chart for this paper.

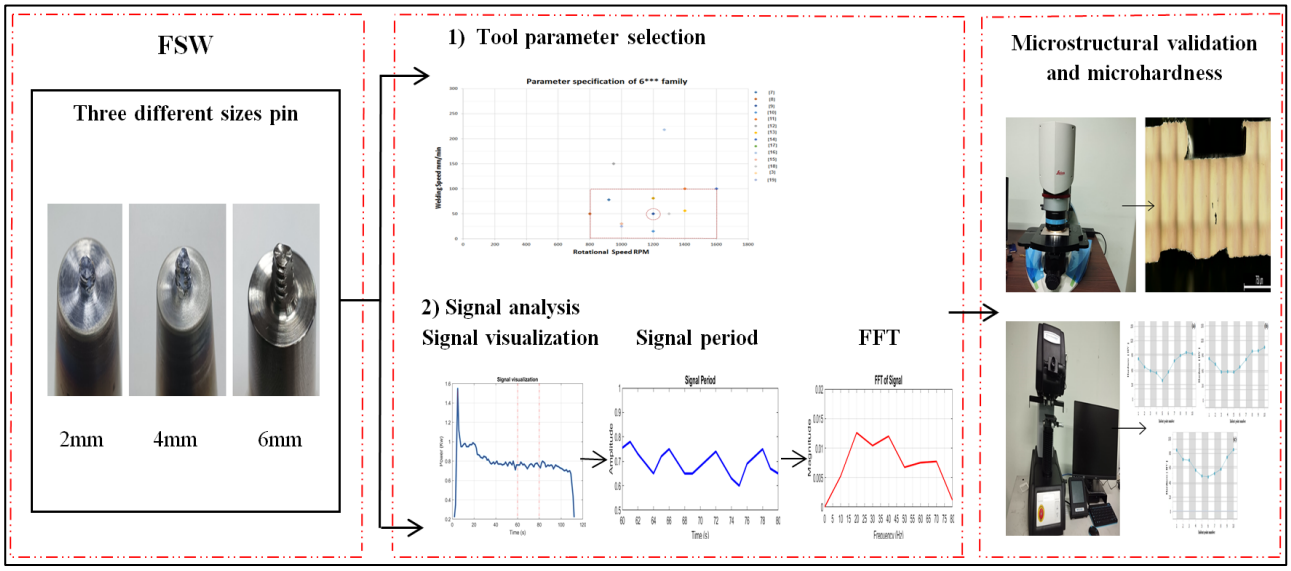

Figure 4. Process signal analysis

Vickers hardness and microstructure testing were conducted to evaluate mechanical integrity. The weld area was sectioned and tested from the most affected zone on both top and bottom surfaces. Results were used to correlate signal features with weld strength. The evaluation of weld external and internal conditions is an important means of studying the influence of operating parameters, the welding process, and the selected material. Thus, the workpiece welded material is tested using power and vibration signals. These signals are analyzed to identify the weakest portion of the welding path. The signals are evaluated at a specific distance from the pin tool path joint. The distance is measured at the affected area to assess quality and mechanical properties.

3. Results and Discussion

Time-domain analysis revealed variations in vibration and power signal characteristics based on pin size and material thickness. The results for each tool and each pin size were recorded during the bottom FSW on similar material. For the three constant welding parameters and different aluminum alloy thickness plates, with the pin length 2 mm longer than the plunge-in depth force, the weld quality assessment of vibration and power is shown in Figure 5 for the time-domain signal.

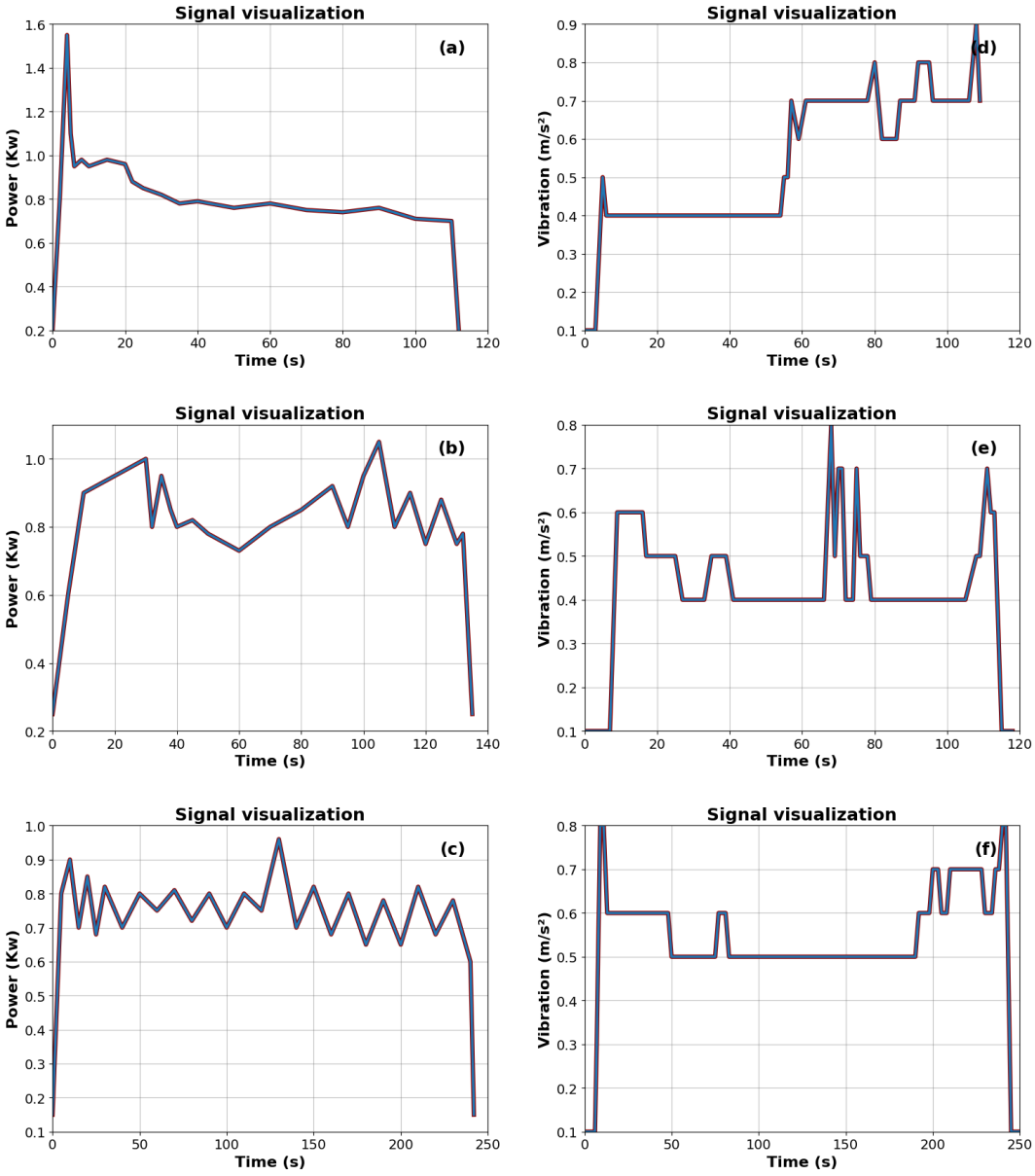

Figure 5. Comparison of power and vibration signal bottom welding for three different pin sizes tools (a-d) 2 mm, (b-e) 4 mm, (c-f) 6 mm in the time domain, respectively

The trend of the power signal over time reveals the FSW's different stages along the welding path. In Figures 5(a-c), the measured power of the 2 mm pin indicates energy consumption during welding. During the first stage of plunging, the tool has a higher start-load signal, which increases its initial rotational speed. The plunging power has less spick load during preheating, but continues a stable decrease during the friction stir welding stage. However, the tool's exit has reset the load to the minimum again. On the other hand, the 4 mm and 6 mm tool sizes show a lower-power signal profile during the travelling phase. It was observed that the larger tool size decreases the peak load with increasing thickness. It was also found that the tapered with three flats and thread pin profile has fewer surface flash defects in 6 mm pin-size material than the tool with 2 mm and 4 mm sizes. The previous result showed that the 2 mm pin produced the highest peak in the main frequency of the power signal, which is 6 kN higher than that of the 6 mm pin. These results show that the largest tool size has the fewest internal and external weld defects, due to greater material stability. Moreover, different weld vibration signals were analyzed in the time domain. In Figures 5(d-f), the measured 2 mm tool size produces lower-frequency vibrations at the first stage of welding. The other welding stages are not very different compared to the power load signal during the dwelling phase. However, it shows a gradual increase in the third-stage welding stage across all tool sizes. As the material thickness increases, the welded material's vibration increases, leading to greater machine vibration. This increase in vibration is due to a tool pin defect on the specimen. The defective side of the material is causing higher signal spikes during welding. The final stage is reached with different exit-stage values due to the specific time limit imposed during welding. The assessment of the pin tool size revealed that the low-size pin has the highest vibration of 0.9 m/s², and the external defect caused by submerged material is also the highest. Moreover, the 4 mm plate has the highest vibration dispersion during the bottom welding stage, at 0.8 m/s. The reason is believed to be the availability of material during steering. Compared with time-domain analyses, the 6 mm tool showed the best peak trend.

A larger pin tool size has less effect on welding defects. Also, the third stage shows the greatest change in welding for both signals. This could be the reason the final FFT defect result was extracted for that welding range. Furthermore, the extraction of the tool at the final stage could be analyzed to examine the effects of signal instability in more detail. In this study, the welding stage was used to ensure the accuracy of the power and vibration signals. For that reason, the FFT analysis will reveal the internal defect welds in the frequency domain, as well as power and vibration.

3.1 Power Signal Analysis

Frequency-domain evaluation refers to the process of analyzing vibration and power signals not only over time but also in terms of their frequency content. This allows the signal to detect hidden patterns that may correlate with defects. At a certain distance from the pin tool path junction, the signals are assessed. To evaluate signal accuracy, monitoring, and quality, the distance is measured at the most-impacted area during visual inspection. In this study, the impacted area was within a 100 mm to 133.4 mm distance from the start location that was cut from each of three 6061AA joints welded. Power signals were measured over a 60-s to 80-s time window. After that, the power features corresponding to the sample's position were also extracted for further analysis. These features indicate the distribution of the affected area along the welding path. Figure 6 shows the extraction of information from the impacted area in the weld joint for the power signal. Similarly, the power signal location has been selected in the same impacted area for all welded materials. In order to detect the defect of the power signal analysis of 2 mm butt welding in one selected area. The power signal is assembled by four stages of the FSW process: plunging, dwelling, welding, and extracting. The plunging stage starts from 0 s and ends at 5 s. During this time, the power increased gradually, very rapidly, to a maximum of 1.55 kW, then decreased in the dwelling stage for 4 s to an average of 0.95 kW. The welding stage remains stable for 100 s, with a slight downward trend. During the extraction stage, the power suddenly decreased to approximately 0 kW in 4 s, as shown in Figure 7(a). Meanwhile, a specific area of the signal has been taken to mark the power wave frequency in one of the defective segments on the path weld. The period was measured within 20 s, which yielded 3 s, 6 s, and 3 s wave oscillations. The highest oscillation is 0.79 kW, as shown in Figure 7(b). In Figure 7 (c), the FFT converts the waveform signal from the time domain to the frequency domain. It is an approach that represents the data in the defective area across specific areas and frequency domains. This approach simplifies the detected defect into signal peaks, aiding in understanding the data. Finally, Figure 7(d) shows the microstructure of the joint morphology-defective part, marked in red, and the time-domain periodic oscillation distance on the top surface. The mark is structured in the stirring zone SZ to show the change in specific period width of 33 mm, equivalent to 20 s of rotational speed along the welding path.

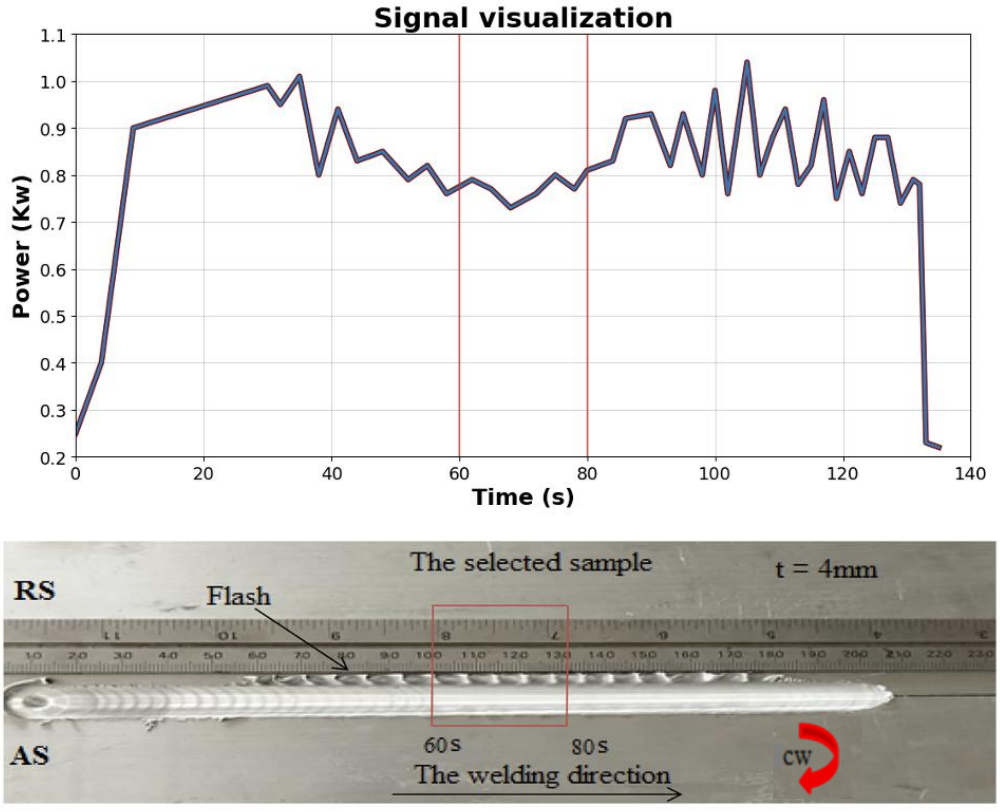

Figure 6. The location of the selected power signal and the defective sample area of a 4 mm pin size, bottom welding

The previous results illustrate that the power signal can detect the defect in one selected area of the joint. Hence, this segment shows a defective microstructure ratio of 90.63% between the first and second harmonics in the frequency domain. This result is considered significant compared with W. Guan et al., who reported defect identification of force signals with an accuracy of 96.43% [8]. Moreover, it was noted that the 6 mm pin produces the best sound weld among

the tool types, at 0.72 kW. Its shape also facilitates easier material flow during friction stir welding, resulting in a gradual decrease in surface defects along the welded path. While the internal section of 2 mm pin size is shown, a better value of 0.76 kW is observed compared to the 4 mm pin with 0.78 kW at the cut-welded section of 60s period. The 2 mm defective area was taken with 20 s, which produced a 3 s, 6 s, and 3 s wave oscillation, and cut at the initial part at peak heights of 0.79 kW. The FFT and microstructure yield identical results, with a period width of 33 mm for shallow holes and voids. In contrast, the larger 4 mm pin size results in increased defect occurrence due to greater material interaction and plastic deformation. The defective 4 mm and 6 mm joint area was selected at 20 s, with wave oscillation times of 10, 2, 3 s, and 5, 4, 2 s, and wave heights of 0.78 kW and 0.72 kW in sequence. Its defective ratios are 45.64% and 44.29%, in that order. The FFT and microstructure show identical results with a period width of 33 mm, corresponding to the welding speed period width. The differences among the three sizes of tool pin power signal analyses for the top and bottom areas are shown in Table 2. Also, the statistical time-domain analysis shows the highest mean, median, standard deviation, and kurtosis with values of 122.5, 123, 70.3, and 3.1×10^9, respectively, for a 6 mm pin. The least data is found for the 4 mm pin size in the Y direction, but not for the 2 mm pin size in the X direction. It has been observed that the X-direction data is higher in most front-welding cases.

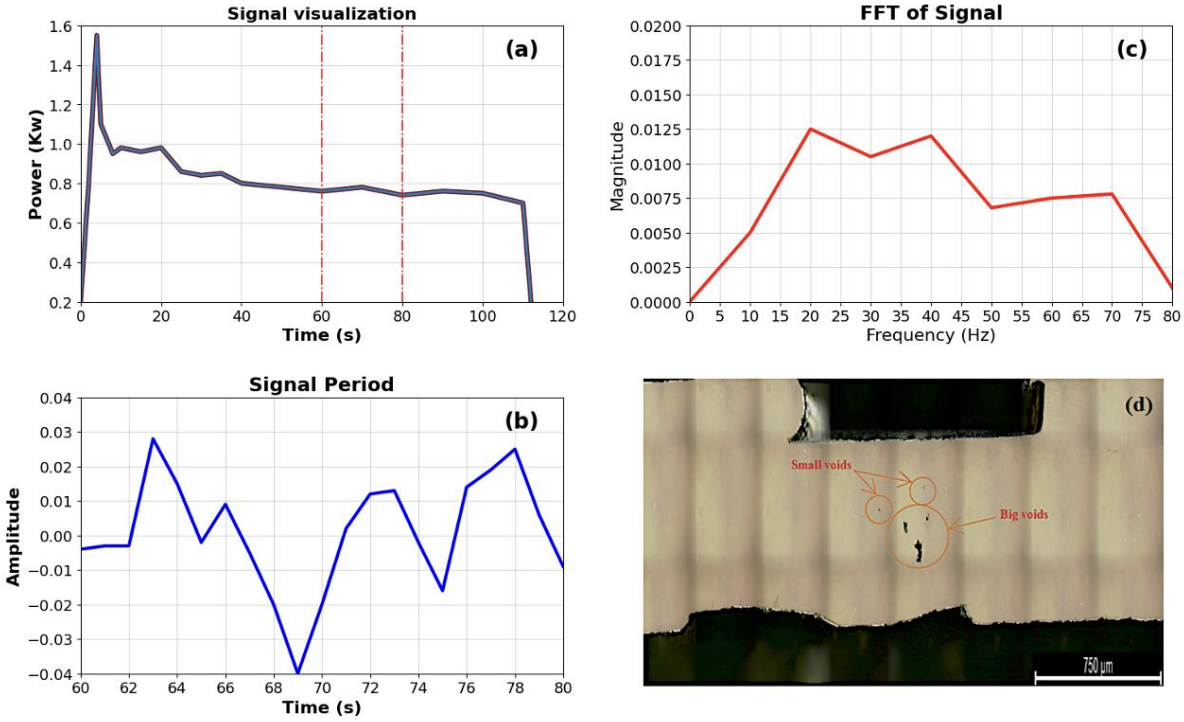

Figure 7. The power signal analysis of 2 mm butt welding : (a) The power signal versus time (b) the selected defective area (c) FFT frequency domain in power signal (d) the surface morphology of the 2 mm pin size joint

To sum up, the correlation between the first higher-harmonic peaks in the power signal and the defect can be calculated using equation 4. The defect ratio equals the D parameter of the first and second higher signals. The first harmonic in the FFT (frequency domain) corresponds to a tool rotation of 1200 RPM, or 20 Hz. The presence of the defect ratio can be directly validated using microstructural and hardness tests. In this study, the bottom welding was explained in more detail. However, weld quality can also be predicted using other welding parameters. For example, the defect created can be weaker at different rotational and welding speeds. On the other hand, this result is obtained with a selected range of the most studied using constant welding parameters. The bottom weld analysis revealed that smaller pins have a higher FFT frequency ratio in the power signal, with a value of 90.63%. Moreover, the 4 mm joints exhibit a significant void defect ratio of 45.64%. In contrast, the 6 mm pin size yielded the smallest defect size, with a ratio of 44.29% in the FFT analysis. This finding is closely linked to the microstructure-void size results and to overall weld quality. The weld quality will be further validated using hardness measurements along the welding path, which are influenced by the tool pin profile and material thickness. This work demonstrates that weld quality can be influenced by various factors, including material thickness, which may also affect joint strength. Thicker materials can enhance the weld's strength as the tool contacts the workpiece. From Table 2, the 2 mm pin showed the highest peak amplitude, indicating the highest resistance. FFT analysis confirmed that the 2 mm pin also produced the highest dominant frequency amplitudes, approximately 6% higher than those of the 6 mm pin. It also indicates that smaller pin sizes induce greater vibration, likely due to increased tool-workpiece interaction and low stability of small workpieces. The higher vibration leads to a higher amplitude of the trend of the defect signal that accrues. This result will be demonstrated in the next subsection.

Table 2. kW comparison of the three different pin sizes

Face welded Pin size	Power signal and impacted area for top welding	Power signal and impacted area for bottom welding
2 mm	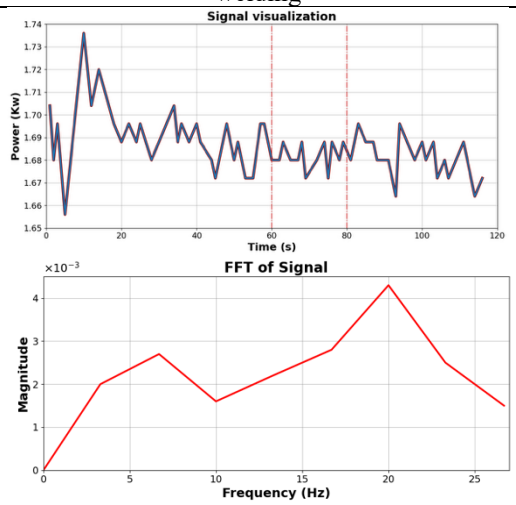	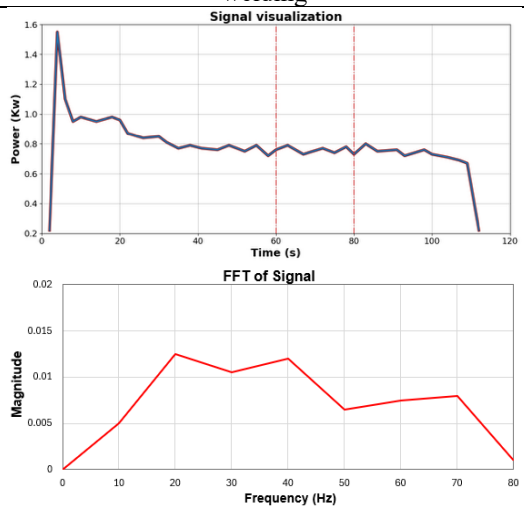
4 mm	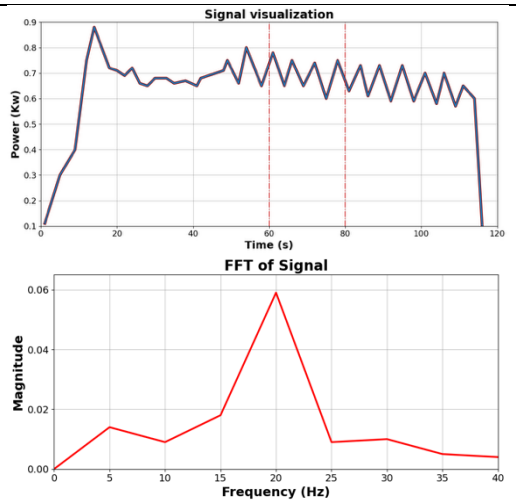	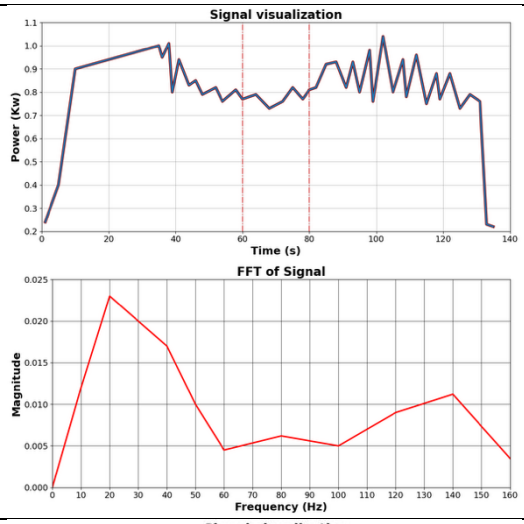
6 mm	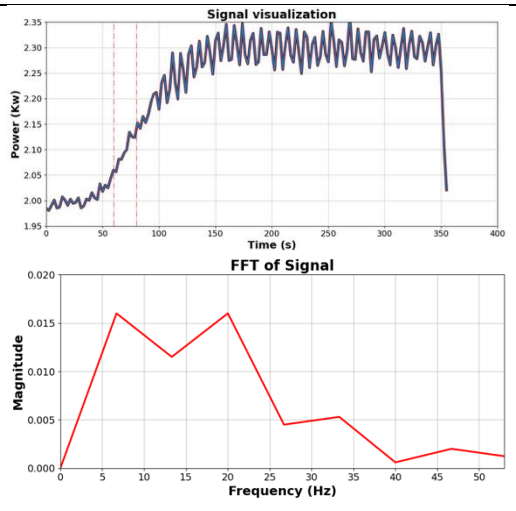	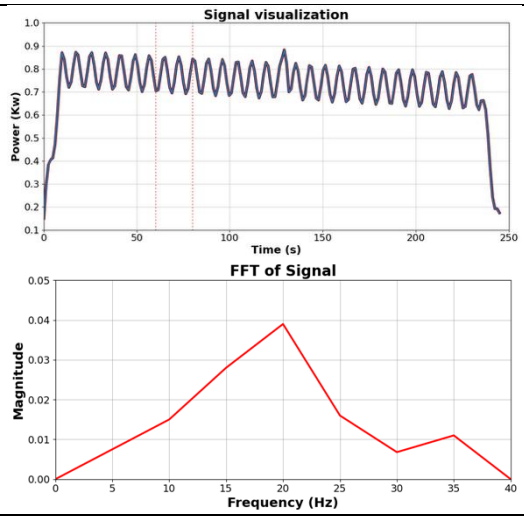

3.2 Vibration Signal Analysis

A good understanding of how CNC machines behave when vibrating allows engineers to start thinking about launching a highly sensitive instrument or about detecting ways to produce a product (material) safely. Vibration signals contain a lot of important information about the operating state of mechanical equipment, but they are affected by noise, interference, and other factors. Model vibration analyses of defects detected in the weld are usually performed in the time and frequency domains. Frequency-domain analysis is one of the most widely used methods for mechanical fault diagnosis and signal processing [32]. The reason for that is the time-domain limitation in the process analysis. Some

important features are obscured or lost, so the time-domain features cannot fully capture the signal's information. The Fourier transform is a signal analysis approach that indicates the frequency characteristics of the undesirable welded places (defects). It provides an important basis for extracting features in the time–frequency domain characteristics of the pin tool about FSW. The FFT converts the collected process vibration signal to the frequency domain. The features of the welding vibration frequency-domain signals at different frequency locations are identified. In addition, the filter removes the noise. The following are the formulas for calculating the high-pass and low-pass filters of noise [33]:

$$y_{HighPassFilter}(k) = \sum n\, x(n) \cdot g(2k - n) \tag{6}$$

$$y_{LowPassFilter}(k) = \sum n\, x(n) \cdot h(2k - n) \tag{7}$$

The features of the weld in this paper are identified in a specific area using an FFT analysis to detect internal defects in the filtered signal. The analysis of the vibration bottom weld of a 2 mm pin at distances of 60 s to 80 s is shown in Figure 8. In Figure 8(a), the welding vibrations versus time during the four phases are displayed. The vibration increases gradually throughout the plunging phase as the pin plunges into the plate to 0.5 m/s^2. Then, the dwelling phase continuously generates heat to soften the materials, leading to a slight decrease in the vibration peak value to 0.4 m/s^2, followed by a sudden increase from 0.4 to 0.9 m/s^2 for 50 s starting at 55 s time value, which is due to the rise of vibration generation and results in some flash around the weld path. After that, the retracting phase drops the value to 0.7 m/s^2 due to less resistance at the end-welded area. Next, with a 20 s signal period, the surface pin tool travel phase was analyzed in the time domain, as shown in Figure 8(b). In Figure 8(c), the signal period is also analyzed in the frequency domain. During the analysis, the FFT was used to transform and detect changes in the material during welding; the vibration signals were not fully visualized. Therefore, a low-pass filter is used to eliminate high-frequency content, resulting in a noise-signal interface as shown in Figure 8(d). The filtered FFT shows the first-highest vibration peak at 20 Hz with a value of 0.1239, indicating a high amplitude. The second-harmonic peak is 0.0462, followed by three peaks for the defective joint configuration.

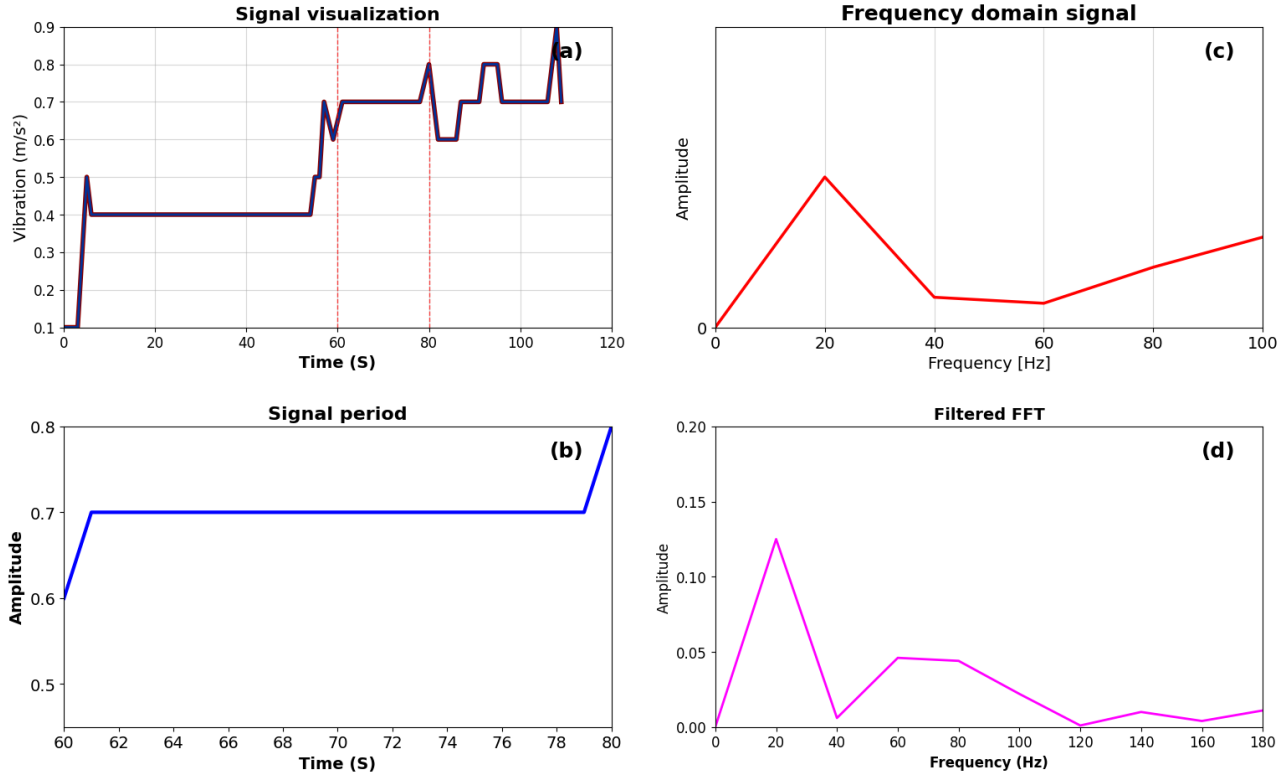

Figure 8. The vibration signal analysis of 2 mm butt welding : (a) The vibration signal versus time (b) the selected defective area (c) FFT frequency domain in vibration signal (d) The filtered FFT in frequency domain

In addition, the front-side weld has higher material resistance, resulting from a higher plunging vibration phase and slight decreases of 0.1 m/s2 during the dwelling phase. During the travel welding phase, the vibration signal reaches a peak of 0.7 m/s^2. Nevertheless, it drops down to 0.6 m/s^2 at the retracting phase. It indicates that the front welding has lower welding vibration on the front side. Otherwise, the filtered FFT amplitude value is 0.1239 high at the first peak. The second-harmonic peak is 0.0462, corresponding to 24.4%. It indicates that the defect is created on the front side of the weld. This is mainly because a rough input surface increases the amount of material melted, resulting in insufficient mixing of the plastic materials during the first-run weld, leading to defects. The contributions of eight statistical methods are analyzed in the time domain to reveal the weld pattern. The front weld shows a higher mean and median value of 2.5% of the bottom value. The difference in standard deviation between the two sides is about 1.44, compared to the kurtosis value difference of 322.966$x10^3$. This is because the pin-to-interaction resistance of the first-side weld is lower

than that of the bottom-side weld. This indicates that the vibration defect on the front tool is greater than that on the bottom-side weld. Even though a 4 mm pin size is used on both sides of the welds, there are greater changes in the vibration signal. The front weld also has a higher mean and median of 2.5%, which is the same as a 2 mm pin size. Although the kurtosis is lower for the 2 mm pin size, no difference is observed in the front-side standard deviation. The 6 mm size has shown the highest result compared to the other sizes. The mean and median are presented by 191.5 and 191.5, respectively, in front welding. Meanwhile, the standard deviation and kurtosis are also presented as 110.4 and $285655.603x10^3$, respectively.

Table 3. Comparison of three sizes of pin vibration signal analysis

Face welded Pin size	Vibration signal and impacted area for front welding	Vibration signal and impacted area for back welding
2 mm	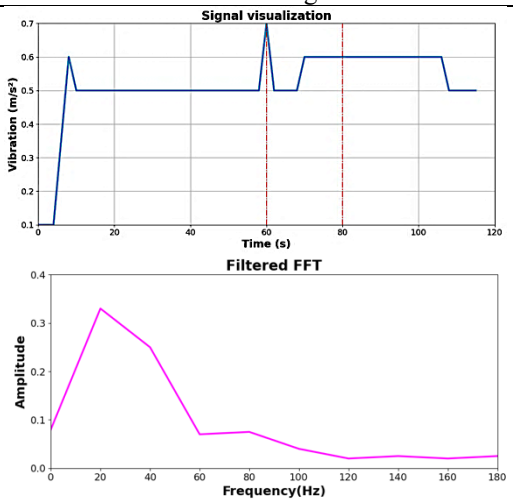	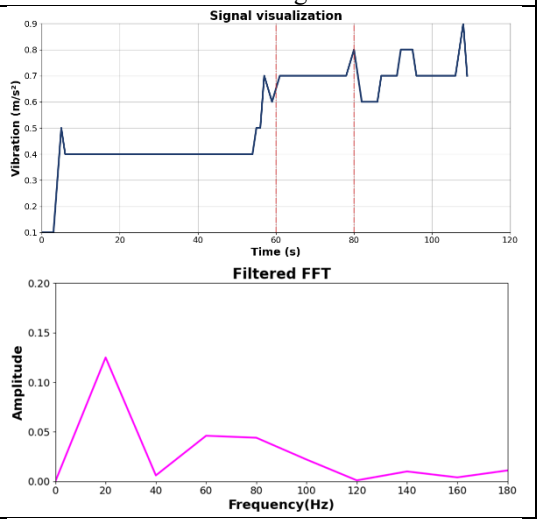
4 mm	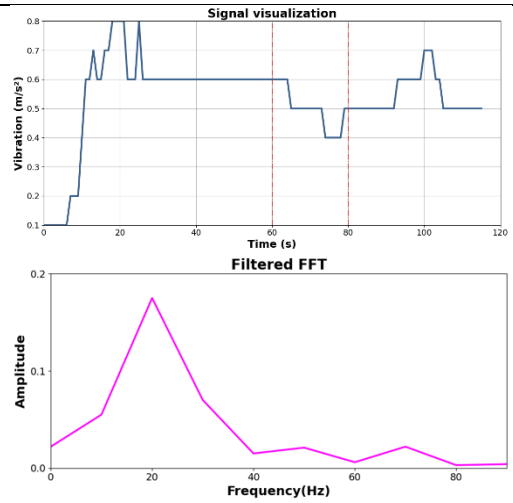	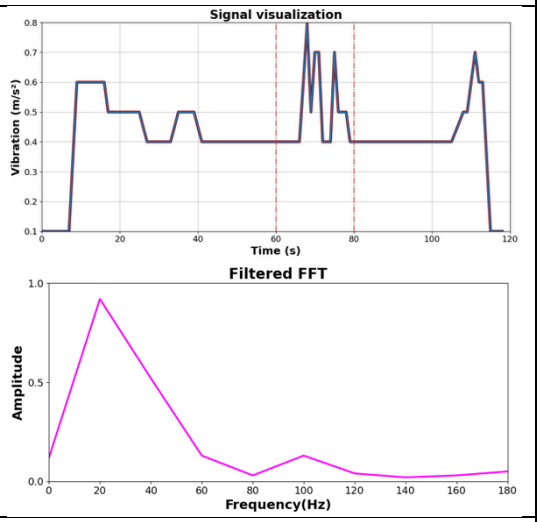
6 mm	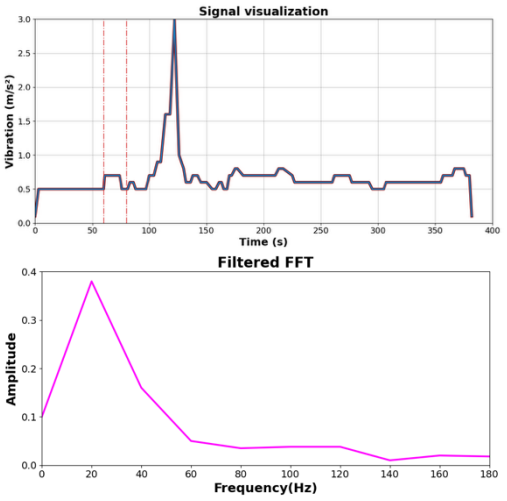	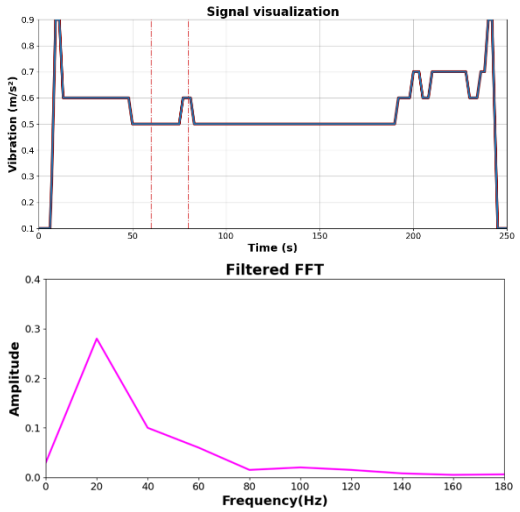

The bottom weld results show a slight decrease in the mean and median to 123.5, but the standard deviation decreases to 71.16. This vibration characteristic is taken in the X direction. Table 3 presents a full comparison of the three pin sizes for time-domain vibration signal analysis and filtered FFT. In addition, the 2 mm time-domain peak magnitude was described as the highest at 0.6 kW in bottom welding. In brief, the best weld of three for the initial value of 60s was 0.4 m/s^2 of a 4 mm pin, but it was not continuous across the weld bath. It is the reason for the poor-quality weld on that pin. Otherwise, the time-domain values for the 6 mm and 2 mm tool sizes are 0.5 m/s2 and 0.6 m/s^2, respectively. The results indicate that a good weld joint corresponds to the microstructure of the defective cut area. All in all, the statistical analysis of the signal characterised the welding trend. The high kurtosis values are particularly > 3 $\times 10^{9)}$, indicating a more stable pattern, which correlates with the 6 mm pin tool. At the same time, the average range standard deviation is between 123.5 and 191.5. It is also noted that the 6 mm pin shows higher vibration, with a defect ratio of 85.10%, which justifies the appearance of voids in the microstructure test. Furthermore, the 4 mm pin exhibited the lowest variation in vibration amplitude, particularly at the bottom plates, suggesting partial stability in the impacted area. Moreover, bottom-surface signals showed increased scattering in the selected materials area, indicating sensitivity to pin condition.

3.3 Macrostructure and Microhardness Measurements

To investigate weld formation and relate the signal pattern, microstructure, and microhardness of Al alloys to mechanical deformation and/or temperature effects in the weld zone (TMAZ/HAZ) [34], these are then measured. For hardness, ten points are taken, and the center points are then calculated. For microstructural analysis, a cross-section of the weld area is cut and observed under the microscope. The defects are usually determined experimentally using an optical microscope or a scanning electron microscope. The structural integrity of the weld is fundamentally related to the geometry and local mechanical properties of the weld zones[16]. The interaction between the tool and the weld material causes the zone-area defect. In this study, the difference in tool sizes for similar welded material integrity and mixed bonding is analyzed. The grain structure indicates whether the welded material combination is of high- or low-strength quality. The grain combination directly affects the welded joints. Mechanical and thermal recrystallization must ultimately result in very fine grains for the highest strength. The grain structures of the transverse welded cross-section after metallographic polishing are analyzed for all welded specimens. Initially, in this work, the welding specimens were cut for microstructural and microhardness testing of the joint using an optical metallographic microscope (Nikon LV150N) and a Vickers microhardness tester, respectively. The microhardness loading rate was 1 kgf, and the indent space was 3 mm from the left edge of the right surface. The weld was cut to assess the quality of the defective areas. The weld strength quality indicator depends on defect size. The pin tools of different sizes vary in their effect on the material strength in the welding zone on the external and internal parts. In Figure 9(a), there is a ribbon flash defect inside the tapered and three flats thread faces of pin-welded material, while the microstructure properties (defect size) are very high compared to the 6 mm pin size. The flash height was midway between the other two pins in some areas. In Figure 9(b), the welded material is affected by a small amount of heat, resulting in a few surface flash defects. The tapered with three flats and thread pin 4 mm shows more peak points in some flash-defective areas and a rough grain structure. When the welding distance of this tool reaches 133 mm, the internal section records the highest flash width. Otherwise, the minimum welding flash width was recorded with the initial welded path. In Figure 9(c), the materials inside the 6 mm welded tool are well mixed, and no defects occur in surface visualization, which is the result of the well-bonded welding of the tapered with three flats and thread pin tool shape. Microstructure testing is measured at a distance of 133 mm from the aluminum weld path and shows the lowest defect area.

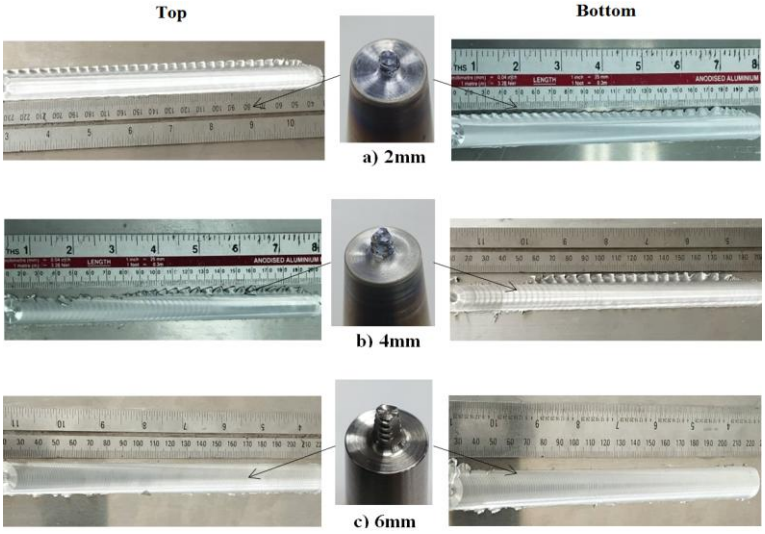

Figure 9. Comparison of the top and bottom weld joints of three different sizes of the pin tool

After testing FSW welds of the 6xxx alloy family, the microstructure and microhardness results show decreases in joint integrity and defect size with reduced welding pin tool size. Furthermore, the welding path is gradually shifted from

the highly affected surface during the small-sized pin weld to the less affected surface during the large-sized weld for the three pin sizes, which is directly related to weld quality. Lastly, microhardness was used to assess strength, and the lowest values were recorded with the 6 mm pin. Also, a minor flash was observed visually; the external section is strongly correlated with vibration and power signals.

3.3.1 Macrostructure inspection

A CNC machine was used to precisely cut and shape a specific area of the welded plate into the required rectangular specimen dimensions. The 60s to 80s rectangle-welded plate areas have been ground into surface shape pieces before polishing for the final optical microstructure test. A macrostructure test is performed on a smooth-surface-finished specimen, and the specimen is visually inspected to be free of defects. The welding parameters are set to be constant across the welding path. The macrostructure of the three pin-sized test specimens is shown in Figure 10.

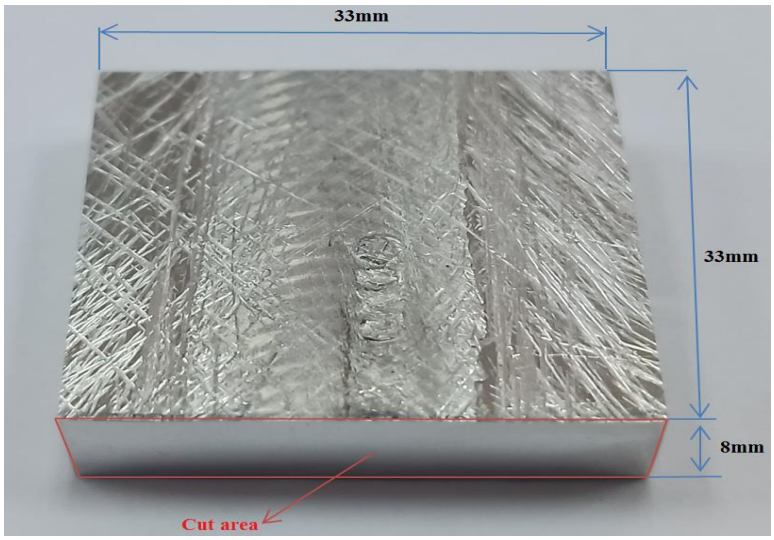

Figure 10. Macrostructure specimen area and dimension

The weld is cut to observe the macrostructure at the defective areas and to evaluate the trial results for three tool sizes, as shown in Figure 11. The larger 6 mm pin size yields the smallest joint voids among the three sizes. This is due to less frictional material flash produced and a uniform (stable) mixed flow. Also, the 6 mm thread pin profile provides sufficient mixing at the chosen welding parameters with lower power consumption. It is observed that the specimen obtained has shallow, big voids and small voids, while the 2 mm and 4 mm specimens develop bigger voids and small voids for both pins. When 4 mm pins rotate, the three flat faces of the pin produce a higher amplitude on the top welded part than on the bottom part due to flash removal. Therefore, the 6 mm pin size produces less energy at the top weld due to less flash, but it increases energy at the back weld because of the double-material connection in the welded part. The good thread of the pin profile also helps form a good microstructure, leading to improved mixing and bonding. The results showed that tool size significantly affects the joint strength of FSW specimens with different material thicknesses.

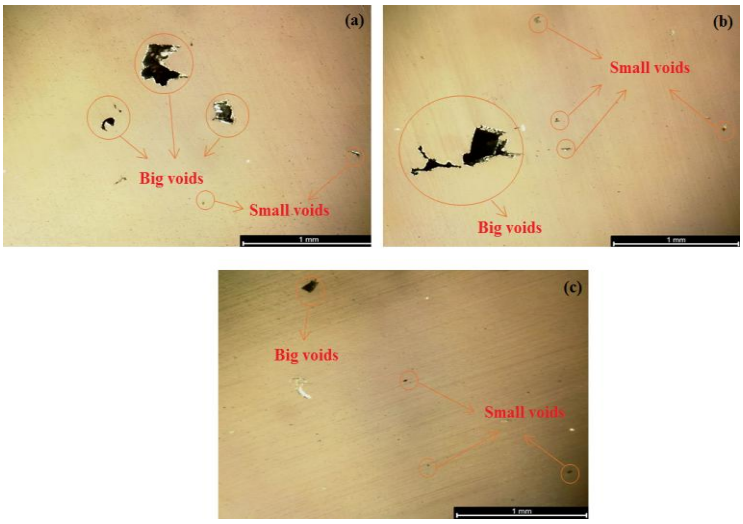

Figure 11. Comparison of the microstructure optical analysis of three different sizes of pin tools: (a) 2 mm, (b) 4 mm, and (c) 6 mm.

After that, the specimen cut joint for each tool size and material thickness is compared and validated against the signals captured by the power and vibration sensors. In addition, the main result of the defective chosen weld was validated at a specific distance. A specific analysis of the power & vibration signals and the microstructure of the FSW joints was conducted to validate the results, as shown in Figure 11. In Figure 11(a), the 2 mm pin size shows different tool influences on the vibration and power signals, as well as on the defect material flow. In addition, the material's thin flash and small width cause changes in the tool's movement. The microstructure optical photo shows a significant decrease in joint mixing in the welding cut area and toward the three large voids along the welding path. In Figure 11(b), the power and vibration signal trends also show an increase in amplitude during the tool welding stage. The trend suggests poor material flow or tool misalignment. The microstructure obtained consists of one large and four small voids on both welded faces; cases typically indicate that specific signal patterns match the weld defect. Figure 11(c) shows the 6 mm increase and the best weld quality. Compared to the other two sizes, the area appears as one large void and three small ones. This result indicates the relationship between the signal and the weld microstructure.

3.3.2 Microhardness test

In this study, the effects of three tool pin sizes, profile, and welding speed on FSW formation have been examined. The microstructure and microhardness reigns were obtained for three material thicknesses. For microstructural analysis, specimens are polished after cleaning the flash to reveal the weld defect zones. Only a few of the flashes are produced at the first visual inspection of the weld. The reason is that the 6061 material is entered via the different pin sizes tool, which results in material debris. From the microtopography, a slightly higher void defect is observed on the weld surface at 2 mm. This is because the rotation path of the welded tool misses the line in the bottom weld in this case. The tool used collects data at the specific centerline of the rotating and welding speeds along the x direction, and it is well centered. However, the three regions produce a good heat distribution and plasticized material. The Vickers microhardness test is performed with a 10 N load and a 10 s test time, according to the machine standard. From the top surface, ten locations in the center cross-section were tested using a microhardness tester. The Vickers indent was created with a spacing of 3 mm to validate the vibration and power signal during the welding process. In Figure 12, microhardness is recorded over a 33 mm area along the weld path, with 10 sample tests. It is found that the weld hardness decreases with decreasing tool size. It has also been found that vibration increases near the tool welding stage and decreases with decreasing hardness. Moreover, the feed rate and rotational speed have no negative effect, as they remain constant across all welding processes. The lowest hardness is recorded at 40 HV for a 2 mm tool, while the 4 mm and 6 mm tools have recorded 60 and 50 HV, respectively. In order, FFT peak amplitudes correlated with hardness values, confirming the reliability of signal features for predicting weld integrity.

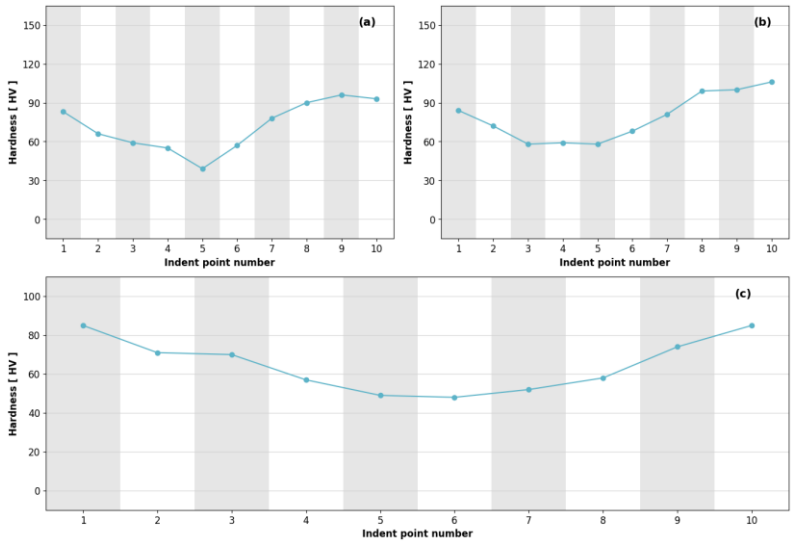

Figure 12. Effect of Micro hardness at three tool sizes at the center line of the specimen (a) 2 mm, (b) 4 mm, and (c) 6 mm

4. Conclusions

This study demonstrates the influence and feasibility of using three different tool pin sizes for inspecting power and vibration defect signals in friction stir welding. The experiment was conducted on similar AA6061 aluminum alloy plates of varying thickness. The power and vibration sensor signals obtained from real-time spindle motor and specimen vibration monitoring during welding were subsequently correlated with the microstructure and microhardness of the welded joint. The material thickness and the pin tool length sizes have different impacts on the power consumed and vibration signals of the FSW machine. These relationships strongly correlate the obtained process signals and the final weld quality and integrity. The main findings from the study are summarized in the following point:

(i) Frequency-domain analysis of the bottom weld revealed that smaller pins exhibit higher FFT power at higher frequencies, indicating a greater presence of defects and underscoring the need for process optimization. The

2 mm and 4 mm joints, which were categorized as thin plates in this study, exhibited significant void defects, with defective microstructure ratios of 90.63% and 45.64%, respectively.

(ii) The 2 mm has produced the highest peak in the main frequency amplitude of the power and vibration signals in the bottom time-domain analysis, with values of 6 kN and 0.9 m/s². It also indicates that the defect is located on the front top side of a 2 mm pin, with 24.4% accuracy in the frequency domain. The reason is likely that there is less material to weld and less energy required than with the other two pin sizes. Moreover, the 6 mm pin size was recorded as the smallest defect size, at 44.29%, in the bottom power frequency domain. This finding effectively connects the time-domain and FFT results to weld quality.

(iii) The 4 mm pin is given the lowest amplitude of about 0.9 m/s² at the main frequency of top-time-domain power welding, because the top material requires less energy to remove flash than the bottom material. Frequency peaks directly correlate to microstructural void defects.

(iv) It is also noted that the 6 mm pin has higher vibration, indicating more work on the 8 mm plate in the FFT. It used less energy in the first weld due to less flash, but it increased the energy in the bottom weld because of the connection of two 4 mm plates to form an 8 mm plate, with a defect ratio of 85.10%, which justifies the appearance of voids in the microstructure test. In order, the 6 mm size has shown the highest result in statistical top analysis compared to the other sizes. Meanwhile, the bottom welds result in slight decreases in the mean, median, and standard deviation.

(v) The result could be further refined by acquiring longer data from more sensitive devices, which would, in turn, undermine the potential effectiveness of simple, economical measurement devices.

(vi) The lowest hardness is recorded at 40 HV with a 2 mm tool, while the 4 mm and 6 mm tools have recorded 60 and 50 HV, respectively. This result revealed that the 2 mm pin produced the least weld strength.

The findings underscore the importance of pin size and characterizations of power and vibration signals, namely FFT amplitudes, for defect detection in the welding process. Future work should include different feature-pinning signal-processing methods for monitoring weld quality and enhanced process control using a sensor-integrated monitoring system, thereby reducing reliance on traditional destructive testing methods.

Acknowledgements
The Authors would also like to thank Universiti Teknikal Malaysia Melaka (UTeM) for all the support.

Funding
This study is funded by the Ministry of Higher Education (MOHE) of Malaysia through Malaysia International Scholarship (MIS) and the Fundamentals Research Grant (FRGS), NoFRGS/1/2023/TK10/UTEM/02/3.

Declaration of Competing Interest
The author declares no conflicts of interest.

CRediT Authorship Contribution Statement
Maged Mustafa Abdulatef: Carry out experimental work, data analysis, and write the paper.
Mohammad Kamil Sued: Supervision, experimental work, idea generation, and writing the paper.
Ahmad Syahrazi Anuar: Data curation and process control.
Tham Sook Chan: Data curation and experiment preparation.
Muhammad Herman Jamaluddin: Involved in equipment setup and preparation.
Ahmad Zaki Hj Shukor: Involved in data acquisition and sensor calibration.
Mohd Khairi Mohd Zambri: Contribute to process monitoring and ideas for data measurement.
Nor Azazi Ngatiman: Supervision in signal vibration, software analysis, and data analysis.

Availability of Data and Materials
The data supporting this study's findings are available on request from the corresponding author.

Ethics Declarations
This study did not involve human participants or animals. Ethical approval was therefore not required.

Generative Artificial Intelligence Declarations
The authors claim that artificially intelligent-assisted technologies, such as generative AI, were not used to generate content, ideas, or theories. We have just utilized AI to enhance readability and refine the language. This was used with extreme human control and oversight. The authors take full responsibility for reviewing and approving the content.

References

[1] Y. Wang, T. Gao, D. Liu, H. Sun, B. Miao, X. Qing, "Propagation characteristics of ultrasonic weld-guided waves in Friction stir welding joint of the same material," *Ultrasonics*, vol. 102, p. 106058, 2020.

[2] M. Ali, S. Mustapha, J. Tarraf, G. Ayoub, R. Hamade, "Detection and assessment of flaws in friction stir welded joints using ultrasonic guided waves : experimental and finite element analysis," *Mechanical Systems and Signal Processing*, vol. 101, pp. 516–534, 2018.

[3] L. Trueba, G. Heredia, D. Rybicki, L.B. Johannes, " Effect of tool shoulder features on defects and tensile properties of friction stir welded aluminum 6061-T6," Journal of Materials Processing Technology vol. 219, pp. 271–277, 2015.
[4] A. Baraka, G. Panoutsos, S. Cater, "Technical paper A real-time quality monitoring framework for steel friction stir welding using computational intelligence," *Journal of Manufacturing Processes*, vol. 20, pp. 137–148, 2015.
[5] B. Das, S. Bag, S. Pal, "Defect detection in friction stir welding process through characterization of signals by fractal dimension," *Manufacturing Letters*, vol. 7, pp. 6–10, 2016.
[6] S.A. Teresa, C. Ersilia, D.E.A. Giorgio, "Monitoring of the friction stir welding process: A preliminary study," *Materials Research Proceedings*, vol. 41, pp. 2891–2900, 2024.
[7] J. Kouguchi, H. Yoshioka, "Monitoring method of cutting forces and vibrations by using frequency separation of acceleration sensor signals during milling process with small ball end mills," *Precision Engineering*, vol. 85, 2023, pp. 337–356, 2024.
[8] W. Guan, D Li, L Cui, D Wang, "Detection of tunnel defects in friction stir welded aluminum alloy joints based on the in-situ force signal," *Journal of Manufacturing Processes*, vol. 71, pp. 1–11, 2021.
[9] D. Akmaz, "A new signal processing approach/method for classification of power quality disturbances," *Digital Signal Processing*, vol. 130, p. 103701, 2022.
[10] D. Mishra, R. Basu, S. Dutta, S.K. Pal, D. Chakravarty, "A review on sensor-based monitoring and control of friction stir welding process and a roadmap to Industry 4 .0," *Journal of Manufacturing Processes*, vol. 36, pp. 373–397, 2018.
[11] M. Akbari, M. Esfandiar, and A. Abdollahzadeh, "The role of force and torque in friction stir welding : A detailed review," *Journal of Advanced Joining Processes,* vol. 11, p. 100289, 2025.
[12] K. Balachandar, R. Jegadeeshwaran, D. Gandhikumar, " Condition monitoring of FSW tool using vibration analysis – A machine learning approach," *Materials Today : Proceedings*, vol. 27, pp. 2970–2974, 2020.
[13] S.S. Kumar, S.D. Ashok, S. Narayanan, "Investigation of friction stir butt welded aluminium alloy flat plates using spindle motor current monitoring method," *Procedia Engineering*, vol. 64, pp. 915–925, 2013.
[14] G.H. Kumar, B. Vishwanath, R. Purohit, R.S. Rana, "Mechanical behaviour of friction stir welding on aluminium based composite material," *Materials Today: Proceedings,* vol. 4, no. 4, pp. 5336–5343, 2017.
[15] M. Syahid, M. Ashraf, K. Moghadasi, S. Raja "Recent research progress in friction stir welding of aluminium and copper dissimilar joint : a review," *Journal of Materials Research and Technology*, vol. 15, pp. 2735–2780, 2021.
[16] W. Guan, L. Cui, H. Liang, D. Wang, Y. Huang, M. Li, "The response of force characteristic to weld-forming process in friction stir welding assisted by machine learning," *International Journal of Mechanical Sciences*, vol. 253, p. 108409, 2023.
[17] B.A. McWilliams, J.H. Yu, C. Yen, " A numerical simulation and experimental characterization of friction stir welding on thick aluminum alloy aa2139-t8 plates," *Materials Science and Engineering: A*, vol. 585, pp. 243–252, 2013.
[18] X.C. Liu, T. Ye, Y.Z. Li, X.J. Pei, Z. Sun, "Quasi-in-situ characterization of microstructure evolution in friction stir welding of aluminum alloy," *Journal of Materials Research and Technology, vol.* 25, pp. 6380-6394*,* 2023.
[19] A. Heidarzadeh, H. Khodaverdizadeh, A. Mahmoudi, E. Nazari, "Tensile behavior of friction stir welded AA 6061-T4 aluminum alloy joints," *Materials & Design*, vol. 37, pp. 166–173, 2012.
[20] P.M.G.P. Moreira, F.M.F. De Oliveira, P.M.S.T. De Castro, "Fatigue behaviour of notched specimens of friction stir welded aluminium alloy 6063-T6," *Journal of Materials Processing Technology*, vol. 207, pp. 283–292, 2008.
[21] M.A. Abdulstaar, K.J. Al-fadhalah, L. Wagner, "Materials Characterization Microstructural variation through weld thickness and mechanical properties of peened friction stir welded 6061 aluminum alloy joints," *Mater. Charact.*, vol. 126, pp. 64–73, 2017.
[22] K.N. Wakchaure, A.G. Thakur, V. Gadakh, A. Kumar, "ScienceDirect Multi-Objective Optimization of Friction Stir Welding of Aluminium Alloy 6082-T6 Using hybrid Taguchi-Grey Relation Analysis- ANN Method," *Mater. Today Proc.*, vol. 5, no. 2, pp. 7150–7159, 2018.
[23] R.V. Rao, M.S. Kumar, "ScienceDirect Experimental Investigation On Effect Of Welding Parameters On The Friction Stir Welding Of AA 6061,"*Material Today Proceedings*, vol. 5, no. 5, pp. 12265–12272, 2018.
[24] D. Maneiah, D. Mishra, K.P. Rao, K.B. Raju, "Materials Today : Proceedings process parameters optimization of friction stir welding for optimum tensile strength in Al 6061-T6 alloy butt welded joints," *Material Today Proceedings*, vol. 27, pp. 904–908, 2020.
[25] S. Azeez, M. Mashinini, E. Akinlabi, "Sustainability of friction stir welded AA6082 plates through post-weld solution heat treatment," *Procedia Manufacturing*, vol. 33, pp. 27–34, 2019.
[26] B. Shailja, A.P.K, P.V. Kumar, "Mechanical and abrasive wear properties of friction stir welded joints of aluminum alloy AA6061-T6 with / without nickel coating," *Strojnícky časopis–Journal of Mechanical Engineering,* vol. 70, no. 2, pp. 21–36, 2020.
[27] I. Dinaharan and R.F. Laubscher, "Predicting the wear rate of AA6082 aluminum surface composites produced by friction stir processing via artificial neural network," *Multidiscipline Modeling in Materials and Structures*, vol. 16, no. 2, pp. 409–423, 2019.
[28] A. Mamgain, A.P. Singh, V. Singh, "Welding investigation on AA 6063-t6 aluminium alloy during friction stir welding process," vol. 35, no. 2, pp. 411–419, 2023.

[29] S. Budin, N.C Maideen, S. Sahudin "Design and development of stirring tool pin profile for reconfigured milling machine to perform friction stir welding process design and development of stirring tool pin profile for reconfigured milling machine to perform friction stir welding process," *Engineering Research Express*, 4 015009, 2022.

[30] H.J. Chauhan, A. Chouhan, S.L. Meena, "Experimental Investigation and Non-Destructive Testing of Friction Stir Welded Aluminium Alloy AA 6082 Using Tool With and Without Shoulder Geometry," *International Research Journal of Engineering and Technology*, vol 3, no. 5, pp. 2656–2664, 2016.

[31] B. Ghosh, H. Das, A. Samanta, J.D. Majumdar, M. Ghosh, "Influence of tool rotational speed on the evolution of microstructure and mechanical properties of precipitation-hardened Aluminium 6061 butt joint during friction stir welding", *Engineering Research Express*, vol. 4, no. 1, p. 015009, 2022.

[32] Y. Wang, S. Zhao, P. Zhang, H. Long, Y. Sun, N. Zhao, "The pin tool wear identification with vibration signal of friction stir lap welding based on a new pin tool wear division model," *Measurement*, vol. 242, p. 116131, 2025.

[33] T.W. Liao, J. Roberts, M.A. Wahab, A.M. Okeil, "Building a multi-signal, multi-signal-based defect prediction system for a friction stir welding process," *Procedia Manufacturing*, vol. 38, no. 2019, pp. 1775–1791, 2020.

[34] A.F.S. Bugarin, C.P. De Abreu, M. Terada, H.G. De Melo, I. Costa, "Effect of friction stir welding (FSW) on the electrochemical behavior and galvanic coupling of AA2024-T3 and AA7475-T651,"*Materials Today Communications*, vol. 25, no. April, p. 101591, 2020.